RUSSELL, L., GLEESON, D. A., MINOGIN, V. G. & NIC CHORMAIC, S. 2009. Spectral distribution of atomic fluorescence coupled into an optical nanofibre. *Journal of Physics B: Atomic, Molecular and Optical Physics*, 42(18), 185006.
doi: 10.1088/0953-4075/42/18/185006

Spectral distribution of atomic fluorescence coupled into an optical nanofiber

Laura Russell,[a,b,] Daniel A. Gleeson,[a,b,] Vladimir G. Minogin,[b,c,d] and Síle Nic Chormaic[a,b*]

[a] *Physics Department, University College Cork, Cork, Ireland.*

[b] *Photonics Centre, Tyndall National Institute, Cork, Ireland.*

[c] *Institute of Spectroscopy Russ. Ac. of Sciences,*

142190 Troitsk, Moscow region, Russia.

[d] *Dept. of Applied Physics and Instrumentation,*

Cork Institute of Technology, Cork, Ireland.

(Dated: February 17, 2009)

Abstract

We analyze the lineshape of the fluorescence emitted by a cloud of optically excited cold atoms coupled into an optical nanofiber. We examine the efficiency of the fluorescence coupling and describe the asymmetry of the lineshape caused by the red-shift arising from both the van der Waals and Casimir-Polder interaction of the atoms with the surface of the optical nanofiber. We conclude that the lineshape of the fluorescence coupled into an optical nanofiber is generally influenced by van der Waals and Casimir-Polder redshifts and, although the contribution from the Casimir-Polder effect is small, both effects should be considered for a complete evaluation.

PACS numbers: PACS: 34.35.+a, 32.70.Jz, 32.70.Fw

*Electronic address: s.nicchormaic@ucc.ie

I. INTRODUCTION

During the past decade there has been considerable interest in analyzing the interaction between optically excited cold atoms and dielectric nanobodies. One important aspect of such an interaction is the resultant modification of the spontaneous emission rate of atoms located near nanobodies, such as dielectric nanofibers, nanospheres and nanodisks [1–4]. Fluorescence radiation emitted by excited atoms located near the nanobody and, subsequently, coupled *into* the nanobody [5, 6] is another practically important aspect that should be considered. An experimental observation of the optical coupling efficiency in such an "atom & nanobody" system, and the spectral dependence of the fluorescence intensity coupled into the dielectric nanobody, may yield information about the interaction strength between the atoms and the nanobody surface, including the strengths of the van der Waals and Casimir-Polder interactions. The spectral dependence of the coupling efficiency is also of importance for developing schemes for an exchange of quantum information between single atoms, photons, and nanobodies [7, 8]. The problem is of particular significance for developing techniques for trapping cold atoms around optical nanofibers [9–11].

The ability to fabricate optical nanofibers [12, 13] has facilitated the growth of experimental studies into "atom & nanofiber" systems. Recent experimental observations have shown that the fluorescence excitation spectrum may exhibit either a well-pronounced, long red tail [6] or an asymmetry with an increased red wing of the spectral line [14]. In earlier work [6], the long red tail of the spectrum was originally assigned to bound transitions of atoms in the van der Waals potential [15]. However, in later work [14], it was highlighted that the long red tail was only observed when no specific measures were undertaken to clean the surface of the nanofiber prior to data acquisition. Subsequently, on cleaning the surface by violet light, the spectrum exhibited a well-pronounced asymmetry of the spectral line with a prevailing red side [14], rather than the previously reported long red tail.

The above observations clearly show that atom interactions with the surface of a nanofiber may depend strongly on the degree of cleanliness of the nanofiber surface. It is, therefore, of principal importance for experiments on atom-fiber interactions to evaluate the contributions of basic physical mechanisms to the asymmetry of the fluorescent excitation spectrum, rather than the effects of a dirty surface. For clean surfaces, such basic mechanisms include the van der Waals and Casimir-Polder interactions (see, for example, review paper [16]).

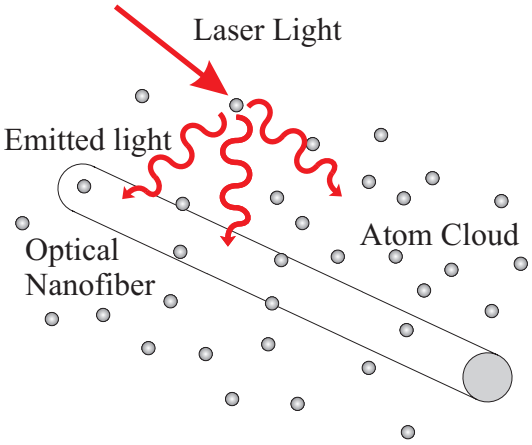

Figure 1: (Color online) Conceptual diagram of the setup with an optical nanofiber surrounded by an atom cloud, optically excited by near-resonant laser light.

The contribution of the van der Waals interaction to the redshift of the spectral line has already been observed in the selective-reflection spectroscopy of cesium vapor located near a dielectric surface [17], for example.

To the best of our knowledge, in the previous works [6, 14, 15] the asymmetry of the coupled fluorescence lineshape was attributed to the redshift caused by the van der Waals interaction alone. In this paper, we evaluate the contributions arising from both van der Waals and Casimir-Polder interactions to the spectral dependence of the coupled fluorescent light and we show that these two basic surface interactions are, in general, responsible for the asymmetry of the lineshape. However, the contribution from the Casimir-Polder effect is very small compared to the van der Waals contribution and may be negligible under certain conditions.

In what follows we analyze the coupling of light emitted by ^{85}Rb and ^{133}Cs cold atomic clouds. We choose ^{85}Rb and ^{133}Cs for our evaluations since these elements are widely used in cold atom experiments. Specifically, we evaluate the fluorescence spectrum emitted by optically excited atoms into the fundamental guided mode of an optical nanofiber. Results from our study show that, for typical radii of optical nanofibers in the range from 200-600 nm, and atomic clouds that are tightly confined around the nanofiber, the fluorescence excitation spectrum exhibits a well-pronounced asymmetry caused by the van der Waals redshift and a slight reduction in the asymmetry arising from the Casimir-Polder redshift.

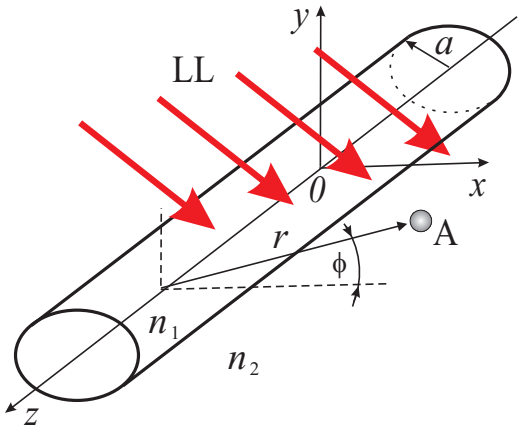

Figure 2: (Color online) Position of the atom (A) near an optical nanofiber and excited by laser light (LL).

II. POWER OF FLUORESCENCE COUPLED INTO THE FIBER

We consider a collection of cold, two-level atoms in the vicinity of an optical nanofiber as shown in Fig. 1. The atoms are excited by a laser field near-resonant to the atomic dipole transition and they emit fluorescent light which partially propagates into the guided modes of the fiber. We consider the case where the frequency of the fluorescent light is below the cut-off frequencies of all modes apart from the fundamental, HE_{11}, mode, so that the fluorescent light can only ever propagate in the fundamental mode. The lower state of the atom is considered to be the ground state and we assume that the upper state can only decay to the ground state. The two-level atom model is partially justified by the fact that, for degenerate optical transitions, different magnetic sublevels have very similar spontaneous decay rates [4].

For a single, motionless, two-level atom placed near the optical fiber and excited by an external laser field near-resonant to the dipole optical transition (c.f. Fig. 2) the probability of finding the atom in the upper excited state is

$$p_{\mathrm{e}} = \frac{1}{2}\frac{\Omega^2}{(\omega-\omega_0)^2+\gamma^2+\Omega^2}, \tag{1}$$

where $\Omega = dE_0/2\hbar$ is the Rabi frequency defined by the atomic dipole matrix element, d, and amplitude, E_0, of the exciting laser field, ω is the frequency of the laser light, ω_0 is the position-dependent atomic transition frequency, and γ is half the position-dependent total spontaneous decay rate, $W_{\mathrm{sp}} = 2\gamma$. In the case we are considering, the spontaneous decay

rate is made up of two position-dependent decay rates, $\gamma^{(g)}$ into the guided modes of the fiber and $\gamma^{(r)}$ into the radiation modes of the fiber, such that

$$W_{sp} = 2\gamma = 2\gamma^{(g)} + 2\gamma^{(r)}. \tag{2}$$

For a single atom the probability of spontaneous photon emission into a guided mode of the fiber per unit time is proportional to the population, p_e, of the excited atomic state and the rate of spontaneous emission, $2\gamma^{(g)}$, into the guided mode,

$$W(r) = 2\gamma^{(g)}(r)p_e(r) = \frac{\gamma^{(g)}(r)\Omega^2}{(\omega - \omega_0(r))^2 + \gamma^2(r) + \Omega^2}. \tag{3}$$

In the above equation we explicitly show that the atomic transition frequency and the spontaneous emission rates are functions of the atom's position, r. For an ensemble of motionless, two-level atoms distributed near the fiber with density $n(\mathbf{r})$, the light power coupled into the fundamental guided mode is accordingly defined by the volume integral

$$P = \hbar\omega \int \frac{\gamma^{(g)}(r)\,\Omega^2}{(\omega - \omega_0(r))^2 + \gamma^2(r) + \Omega^2} n(\mathbf{r})\, dV. \tag{4}$$

Hence, the power coupled into the optical fiber depends on the shape of the atomic cloud and its position with respect to the axis of the fiber. Note that the power considered is the *total* power coupled into the nanofiber. If one were to monitor the power output at one end of the fiber, the observed power would be half the total power.

In the following, we consider the case of a weak optical saturation and neglect the Rabi frequency in the denominator of the excitation probability. At weak saturation the atoms are mostly in the ground state and, as a result, the atomic transition frequency is shifted primarily due to a shift of the ground state. Taking into account that a contribution to the shifts of the atomic states comes from both the van der Waals and Casimir-Polder interactions, the shift of the atomic transition frequency can be evaluated as

$$\omega_0(r) = \omega_0^0 - \delta\omega(r), \tag{5}$$

where $\delta\omega(r)$ represents the shift due to the van der Waals or Casimir-Polder interactions. In the case of a dielectric surface $\delta\omega(r)$ is given by either [16, 18–21]

$$\delta\omega_{vdW}(r) = \frac{C_{3g}}{(r-a)^3}, \tag{6}$$

or

$$\delta\omega_{\mathrm{CP}}\left(r\right)=\frac{3\gamma_{0}}{8\pi}\frac{\varepsilon-1}{\varepsilon+1}\left(\frac{\lambda}{2\pi(r-a)}\right)^{4}\varphi(\varepsilon). \tag{7}$$

In the above equations ω_0^0 is the transition frequency, γ_0 is half the natural linewidth for the free atom, $C_{3\mathrm{g}}$ is the van der Waals constant for the ground atomic state, λ is the wavelength of the laser light, $r-a$ is the distance between the atom and the surface of the fiber, ε is the static relative permittivity of the fiber material, and $\varphi(\varepsilon)$ is a slowly varying function close to unity, $0.77\leq\varphi(\varepsilon)\leq 1$. The explicit structure of the function $\varphi(\varepsilon)$ can be found in [18, 19].

Finally, the total power of the fluorescent light coupled into the guided fiber mode at weak optical saturation can be written as

$$P=\hbar\omega\int\frac{\gamma^{(\mathrm{g})}\left(r\right)\Omega^{2}}{\left[\omega-\omega_{0}^{0}+\delta\omega\left(r\right)\right]^{2}+\gamma^{2}(r)}n\left(\mathbf{r}\right)dV. \tag{8}$$

It is worth noting here that, for a typical dipole transition where the wavelength, λ, lies in the visible to the near-infrared region, the border between the van der Waals and Casimir-Polder interactions usually occurs at a distance from the surface of $r-a\simeq\lambda/10\simeq 50-80$ nm. Van der Waals attractions are very short ranged and contribute primarily at distances very close to the surface, i.e at $r-a\leq\lambda/10$. At larger distances, $r-a\geq\lambda/10$, the Casimir-Polder interaction replaces the van der Waals potential and, therefore, should be included in the evaluations.

A numerical evaluation of the integral defined by Eq.(8) is given in the next section. Before presenting the numerical results, we will briefly discuss the spatial selectivity of the van der Waals and Casimir-Polder interactions and present numerical values of their corresponding redshifts.

Let us assume, for simplicity, that the ensemble of cold, two-level atoms placed around the optical fiber is spatially broad. In principle, every atom could be excited by the laser field and, subsequently, would be able to emit fluorescent light. However, the resonance condition restricts the spatial position of atoms which can, in reality, emit fluorescence. According to Eq.(8), for the case of the van der Waals interaction, the atoms are essentially excited at a mean radial position, $\overline{r}_{\mathrm{vdW}}$, given by

$$\overline{r}_{\mathrm{vdW}}\simeq a+\sqrt[3]{\frac{C_{3\mathrm{g}}}{\omega_{0}^{0}-\omega}} \tag{9}$$

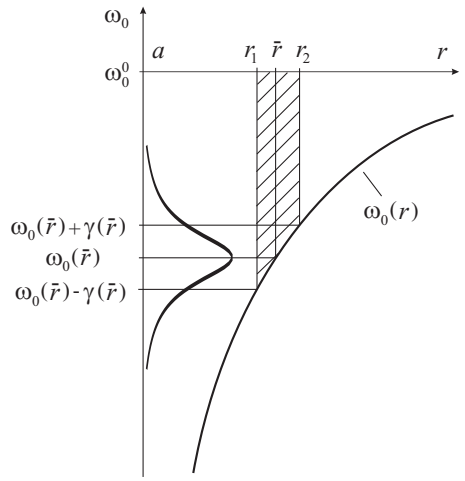

Figure 3: Position-dependent optical absorption line. The shaded area indicates the position of the cylindrical shell containing the excited atoms.

occupying a cylindrical shell coaxially located around the optical fiber as shown in Fig. 3. In a similar way, the Casimir-Polder interaction is responsible for the excitation of atoms in a cylindrical shell with mean radial position, $\overline{r}_{\rm CP}$, given by

$$\overline{r}_{\rm CP} \simeq a + \frac{\lambda}{2\pi}\sqrt[4]{\frac{3\gamma_0}{8\pi\left(\omega_0^0 - \omega\right)}}. \tag{10}$$

The spatial width, δr, of the cylindrical shell containing excited atoms is defined by a position dependent frequency width, $2\gamma(r)$, of an optical resonance. Assuming that at the edges of the shell the probability of atomic excitation is half that at the center of the shell, one can evaluate the radii of the shell edges, r_1 and r_2, as roots of the equations

$$\omega_0\left(r_{1,2}\right) \simeq \omega_0\left(\overline{r}\right) \mp \gamma(r_{1,2}). \tag{11}$$

Hence, the spatial width of the cylindrical shell containing excited atoms is given by $\delta r = r_2 - r_1$. It can be easily shown that, when the average frequency shift, $\omega_0^0 - \omega_0(\overline{r})$, exceeds the natural linewidth, $\gamma(\overline{r})$, the spatial width of the shell is small compared to the shell radii, i.e. $\delta r << r_{1,2}$, and can be evaluated neglecting small variations in the spontaneous emission rate inside the shell, i.e. making the approximation $\gamma(r_{1,2}) \simeq \gamma(\overline{r}) \simeq \gamma_0$. For the van der Waals interaction this simplification results in an estimate of the spatial width of the shell that is given by

$$\delta r_{\rm vdW} \simeq \frac{2(\overline{r}_{\rm vdW} - a)^4\gamma_0}{3C_{3\rm g}}. \tag{12}$$

Table I: Position and width of the cylindrical shell containing excited two-level atoms for van der Waals and Casimir-Polder interactions.

ω	$\omega_0^0 - 2\gamma_0$	$\omega_0^0 - 3\gamma_0$	$\omega_0^0 - 4\gamma_0$
$\overline{r}_{\rm vdW} - a$, nm	74	64	58
$\delta r_{\rm vdW}$, nm	29	16	10
$\overline{r}_{\rm CP} - a$, nm	64	57	53
$\delta r_{\rm CP}$, nm	17	11	7

For the case of the Casimir-Polder interaction the above simplification yields a characteristic width

$$\delta r_{\rm CP} \simeq \frac{2\lambda}{3}\left(\frac{2\pi(\overline{r}_{\rm CP}-a)}{\lambda}\right)^5. \tag{13}$$

The total power of the fluorescent light exciting the guided fiber mode is proportional to the volume, V, of the cylindrical shell with inner radius, r_1, and outer radius, r_2, i.e. the volume $V = \pi\left(r_2^2 - r_1^2\right) l \simeq 2\pi\overline{r}\delta r l$, where l is the spatial extension of the atomic ensemble along the fiber. Hence, the power of the fluorescent light coupled into the guided mode can be evaluated from

$$P = 2\pi\hbar\omega\gamma^{(\rm g)}\left(\overline{r}\right)\frac{\Omega^2}{\gamma^2(\overline{r})}n(\overline{r})\overline{r}\delta r l. \tag{14}$$

For the van der Waals and Casimir-Polder interactions the mean radius and width of the shell containing excited atoms can be estimated from Eqs.(9), (10), (12), and (13).

Numerical values of the mean radii and widths of the shells for the van der Waals and Casimir-Polder interactions for typical optical dipole transition parameters are given in Table I. The data have been calculated for a value of the van der Waals constant, $C_{3\rm g} = 2\pi \cdot 2$ kHz$(\mu$m$)^3$, a wavelength, $\lambda = 800$ nm, and for three values of the laser field frequency, $\omega = \omega_0^0 - n\gamma_0$, with $n = 2, 3, 4$ and $2\gamma_0 = 2\pi \cdot 5$ MHz chosen as a typical value of the natural linewidth for the optical dipole transition. The values shown in Table I indicate clearly that, for a typical dipole transition, both the van der Waals and Casimir-Polder interactions produce comparable contributions to the asymmetry of the fluorescence lineshape.

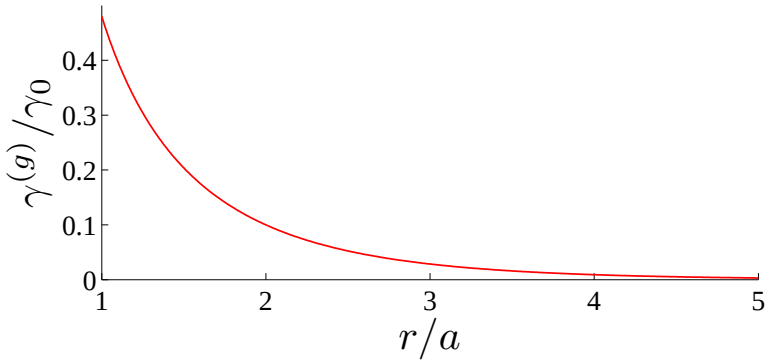

Figure 4: (Color online) Normalized spontaneous decay rate of a two-level atom into the fundamental guided mode, HE_{11}, as a function of distance between the atom and the axis of the optical nanofiber for a radius $a = 200$ nm.

III. NUMERICAL EVALUATIONS

In our basic Eq.(8) there are two unknown quantities: the spontaneous emission rate into the guided mode and the spontaneous emission rate into the radiation modes. Of these two quantities, the most important for our analysis is the rate of spontaneous emission into the guided mode. This quantity varies sharply near the surface of the fiber and, therefore, strongly influences the rate of coupling of spontaneously emitted light into the fiber. The rate of spontaneous emission into the radiation modes changes weakly near the fiber, keeping its value approximately equal to the rate of spontaneous emission into free space. In the following analysis we will neglect the weak spatial dependence of the spontaneous emission rate into the radiation modes and consider only the position dependence of the spontaneous emission rate into the guided mode.

A complete evaluation of the spontaneous emission rate into the fundamental guided mode of an optical fiber is presented in Appendices A and B. The spatial distribution of the evanescent light field of a fundamental guided mode is given in Appendix A, while the spontaneous emission rate into the fundamental mode is given in Appendix B. Figure 4 shows the dependence of the spontaneous decay rate for a two-level atom as a function of distance between the atom and the optical nanofiber surface calculated according to Eq.(B9).

We can now estimate the fluorescence emission line spectrum for ^{85}Rb and ^{133}Cs atoms. We assume the atoms emit fluorescence light into an optical fiber made of fused silica, with

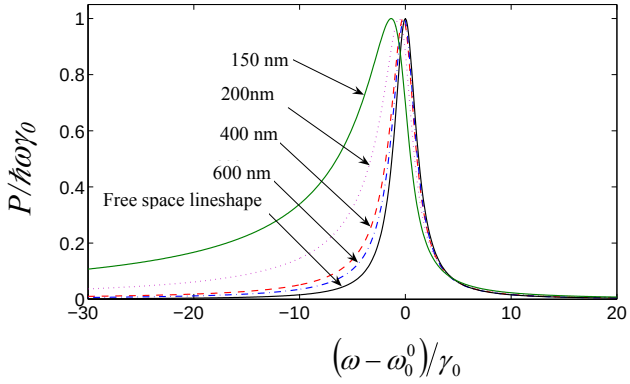

Figure 5: (Color online) Frequency dependence of the fluorescence power from a Rb cloud coupled into the optical nanofiber for a fiber radius $a = 200$ nm and an atomic cloud radius $R = 600$ nm (blue), 400 nm (red), 200 nm (purple), and 150 nm (green). The solid black line shows the free space lineshape and all lines are normalized to a maximum value of 1 for ease of comparison.

permittivity, $\varepsilon = 2.1$. The Rb atoms are assumed to be excited at the 5S-5P optical dipole transition, with a wavelength of 780 nm and a spontaneous decay rate of $2\gamma_0 = 2\pi\cdot$ 6 MHz [22, 23] from the upper 5P state into free space. For the ground state of Rb atoms the van der Waals constant is evaluated as $C_{3g} = 2\pi\cdot 3$ kHz$(\mu$m$)^3$ [17, 24, 25]. Cs atoms are assumed to be excited at the 6S-6P optical transition with a wavelength of 852 nm and a spontaneous decay rate of $2\gamma_0 = 2\pi\cdot$ 5.2 MHz [22] from the upper 6P state into free space. The van der Waals constant for the ground state of Cs atom is $C_{3g} = 2\pi\cdot 1.56$ kHz$(\mu$m$)^3$ [17, 24, 25]. For both optical transitions, with relatively close wavelengths, the refractive index of the fiber is chosen to be $n_1 = 1.45$ and the refractive index of the outside medium is $n_2 = 1$.

We assume that the cold atoms are distributed in a spherically symmetric cloud centered on the axis of the optical fiber. The cloud is assumed to have a Gaussian density distribution, $n(r)$, in the radial direction with half width, R, such that

$$n(\mathbf{r}) = n(r) = \frac{N}{\pi\sqrt{\pi}R^3}\exp\left[-\left(\frac{r}{R}\right)^2\right], \tag{15}$$

where N is the total number of atoms and is given by

$$N = 4\pi\int n(r)r^2dr. \tag{16}$$

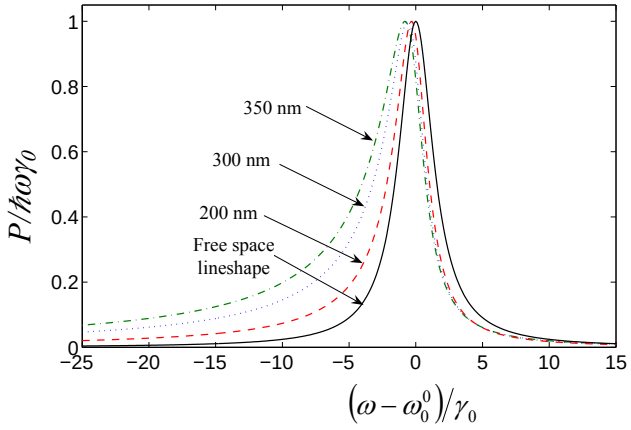

Figure 6: (Color online) Frequency dependence of the fluorescence power from a Cs cloud coupled into the optical nanofiber for a cloud radius $R = 300$ nm and a nanofiber radius of 200 nm (red), 300 nm (blue), and 350 nm (green). The solid black line represents the free space lineshape. All lines are normalized to a maximum value of 1 for ease of comparison.

Figure 5 shows the coupled fluorescence spectrum calculated from Eq.(4) and only taking the van der Waals shift into account for rubidium atoms. As one can see, the asymmetry of the fluorescence lineshape increases when the radius of the atomic cloud decreases. In other words, the tighter the cloud around the fiber the more pronounced the asymmetry becomes. As the radius of the cloud increases the atoms located further from the nanofiber are less influenced by the change in the van der Waals frequency shift and, hence, the shape of the fluorescence spectrum approaches that of the symmetrical, free space distribution.

In Fig. 6 we present the reverse situation for cesium atoms, i.e. the atom cloud size is kept constant while varying the size of the nanofiber. As can be seen, a very similar result is obtained. As we increase the fiber radius, more of the fluorescing atoms are very close to the surface of the fiber and, as a result, the van de Waals potential affects a greater proportion of the total atoms in the cloud, leading to more pronounced asymmetry in the lineshape.

If we now consider a combination of the van der Waals and Casimir-Polder effects we see that a similar phenomenon is observed (c.f. Fig. 7 for cesium atoms). Note that it is not physically realistic to talk in terms of the Casimir-Polder effect on its own; hence, Fig.7 shows a combination of the the van der Waals + Casimir Polder effect for a fixed cloud radius of $R = 400$ nm and varying nanofiber radii. In order to evaluate the total effect, we divided

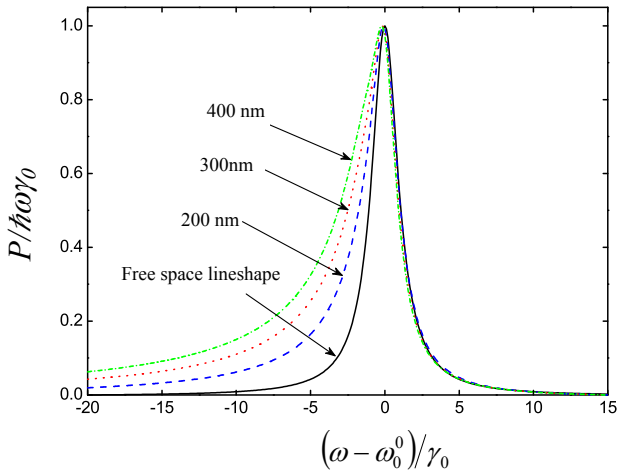

Figure 7: (Color online) Frequency dependence of the fluorescence power from a Cs cloud coupled into the optical nanofiber for redshift contributions from both the van der Waals and Casimir-Polder effects. The cloud radius is $R = 400$ nm and the nanofiber radius is varied. The solid black line shows the free space lineshape and all lines are normalized to a maximum value of 1 for ease of comparison.

the integral into two regions of space, one where the van der Waals effect is dominant and another where the Casimir-Polder effect is dominant. We calculated the total power coupled into the fiber for the corresponding effect in each region and added the results. It is clear that the most pronounced effect is observed when the fiber radius approaches that of the effective cloud radius. This arises since there is a greater population of atoms fluorescing near the fiber surface under such conditions. In the case where the fiber radius and cloud radius are equal, we obtain the most pronounced asymmetry, as illustrated in Fig. 7 for $a = 400$ nm. Note that inclusion of the Casimir-Polder effect has resulted in an overall *reduction* of the redshift to the lineshape compared to that obtained for the van der Waals interaction alone (c.f. Fig. 6).

Since the redshift should be almost entirely due to atoms either on or very near the fiber, the next question to address is whether or not the redshift is due to the van der Waals interaction near the fiber surface, bearing in mind that Casimir-Polder effects are more significant at larger distances and, therefore, may prove to be negligible. Contributions from the Casimir-Polder potential exceed the van der Waals contributions at distances greater

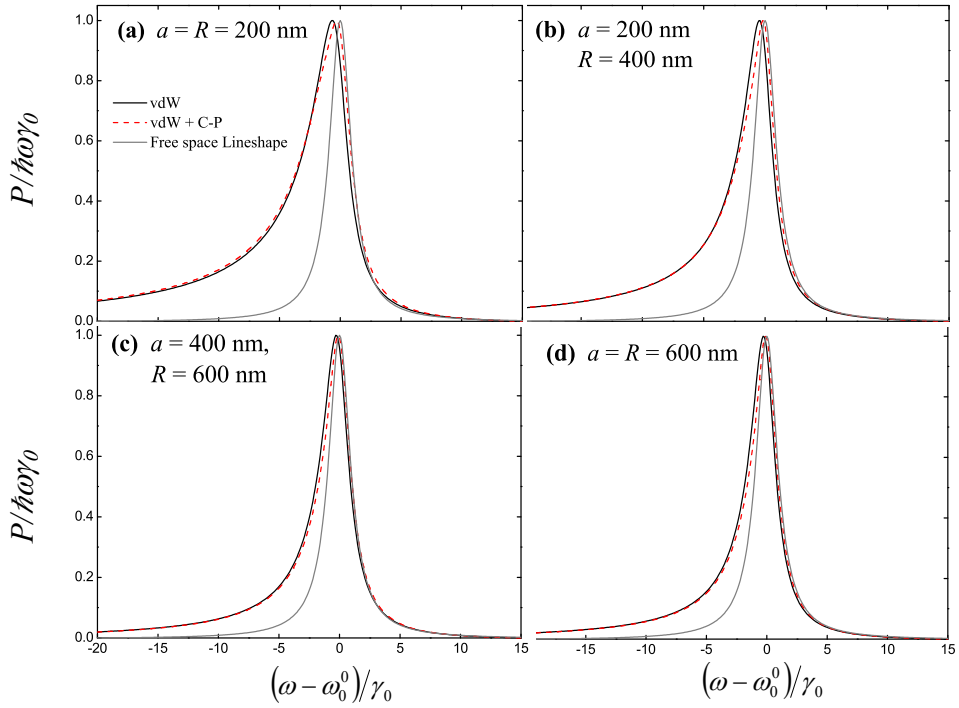

Figure 8: (Color online) Frequency dependence of the fluorescence power from a Cs cloud coupled into the optical nanofiber for different lineshape contributions: van der Waals effect only (black), Casimir-Polder + van der Waals (red), for different cloud radii and fiber radii. All lines are normalized to a maximum value of 1 and the free space lineshape is provided for ease of comparison between the curves.

than 28.3 nm from the fiber for Rb atoms and 67.2 nm for Cs atoms, regardless of the size of the fiber. Despite the fact that this changeover from one regime to another is very close to the fiber, the effect this has on the lineshape of the power coupled into the fiber is relatively insignificant.

The slight reduction in the observable redshift due to inclusion of the Casimir-Polder effect is evident from the plots in Fig. 8. Hence, while the van der Waals interaction is clearly the dominant influence on the lineshape, the overall lineshape should include the contributions from the Casimir-Polder effect in order to obtain a precise prediction of the fluorescence coupled into a nanofiber. A comparative investigation of this behavior for different values of a and R is given, in order to determine under what conditions this change to the lineshape, arising from the Casimir-Polder effect, can be neglected. Clearly, irrespective of the values chosen for a and R, no appreciable difference arises when one includes the Casimir-Polder

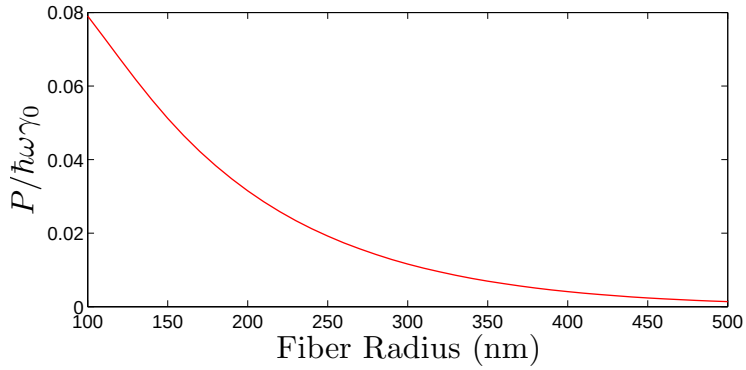

Figure 9: (Color online) Power coupled into a nanofiber as a function of fiber radius. The power shown is the maximum power for each value of fiber radius. The data was plotted for a Rb cloud with $R = 500$ nm.

effect. In fact, we see that the overall redshift decreases with increasing values of a and R. For $a = R = 200$ nm there is a small, but identifiable, difference between the two spectra as shown in Fig. 8(a). For larger values of R with respect to a (Figs. 8(b) and (c)), the difference between the lineshapes reduces as the spectra approach the free space lineshape. Even in the case of $a = R = 600$ nm (Fig. 8(d)), any difference between the two regimes is essentially unresolvable. One explanation behind this result is that when $a = R$ very few atoms experience the Casimir-Polder interaction as the cloud density has decreased by a factor of $\exp^{\left(\frac{a+\lambda/10}{R}\right)^2}$ in the region where Casimir-Polder dominance begins. When $R > a$ the density of atoms has also reduced significantly at the crossover region, thereby yielding a very small contribution to the lineshape from the distant atoms.

Note that, for ease of comparison, we have normalized all powers coupled into the nanofiber to a maximum value of 1 in Figs. 5-8. In reality, there are large differences in the total power coupled into nanofibers of different radii. In Fig. 9 we plot the total power coupled into a nanofiber as a function of nanofiber radius and, as expected, the power reduces significantly with increasing fiber radius for a fixed atom cloud size.

IV. CONCLUSION

We have examined the efficiency of coupling the fluorescence emitted from an ensemble of cold, two-level atoms into an optical nanofiber and we have calculated the frequency

dependence of fluorescence power coupled into the fundamental guided mode of the optical nanofiber. We evaluated the coupled fluorescence spectrum by taking into consideration the two redshifts due to contributions from both van der Waals and Casimir-Polder interactions. Our evaluations show that both the van der Waals and Casimir-Polder potentials contribute to the asymmetry of the fluorescence line and the asymmetry is more pronounced for atomic ensembles that are tightly confined around the optical nanofiber. In the case where the cloud is very much larger than the nanofiber, the contribution from the Casimir-Polder interactions is negligible. We also found that the asymmetry of the fluorescence line increases as the fiber radius is increased. We conclude that for a correct and accurate comparison of the experimentally obtained profile of the lineshape with the theoretical lineshape one should consider both the van der Waals and Casimir-Polder redshifts. This is particularly important if one considers atom clouds that are very tightly confined around the nanofiber. If the power coupled into the fiber were monitored at both ends of the fiber, correlations between the modes emitted in two opposite directions could be studied. This may lead to the possibility of observing photon bunching or anti-bunching.

Acknowledgments

This work was supported in part by Science Foundation Ireland under Grant Nos. 06/W.1/I866 and 07/RFP/PHYF518, and by the Russian Foundation for Basic Research (Project No. 07-02-00748). LR acknowledges support from IRCSET under the Embark Initiative.

Appendix A: Spatial distribution of the electric field for the fundamental guided mode, HE_{11}, of an optical nanofiber

We represent the operator of a quantized vacuum electric field of the guided modes of a nanofiber in a standard form

$$\mathbf{E} = \sum \boldsymbol{\mathcal{E}}_\lambda a_\lambda + \text{h.c.}, \tag{A1}$$

where $\boldsymbol{\mathcal{E}}_\lambda$ is the electric field of a single vacuum guided mode, a_λ is the photon annihilation operator, and index λ describes the direction of propagation and polarization of a single vacuum guided mode. The electric field of a single guided mode can be represented as [26]

$$\boldsymbol{\mathcal{E}}_\lambda = i\sqrt{\frac{\hbar\omega_\lambda}{2\varepsilon_0 L}}\,\widetilde{\mathbf{e}}_\lambda \mathrm{e}^{i\beta_\lambda z + im\varphi}, \tag{A2}$$

where ω_λ is a mode frequency, β_λ is a propagation constant, $\widetilde{\mathbf{e}}_\lambda = \widetilde{\mathbf{e}}_\lambda(r,\phi)$ is a normalized amplitude of the electric field, m is a quantum number of the mode angular momentum, and L is the length of a one-dimensional "box" which is defined by a spatial periodicity of the field. The electric field amplitude of a single guided mode is normalized as

$$\int_0^{2\pi}\int_0^{\infty} n^2(r)\left|\widetilde{\mathbf{e}}_\lambda\right|^2 d\varphi r dr = 1, \tag{A3}$$

where $n(r)$ is the value of the refractive index equal to n_1 inside the fiber and $n_2 = 1$ outside the fiber. The above representation of the vacuum field corresponds to a standard form of the vacuum field Hamiltonian

$$H_{\text{vac}} = 2\varepsilon_0\varepsilon\sum\int dV\left|\boldsymbol{\mathcal{E}}_\lambda\right|^2\left(a_\lambda^\dagger a_\lambda + \tfrac{1}{2}\right) = \sum\hbar\omega_\lambda\left(a_\lambda^\dagger a_\lambda + \tfrac{1}{2}\right). \tag{A4}$$

For the fundamental guided mode, HE_{11}, the propagation constant β is defined by the eigenvalue equation as

$$\begin{aligned}\frac{J_0(ha)}{haJ_1(ha)} = &-\left(\frac{n_1^2+n_2^2}{2n_1^2}\right)\frac{K_1'(qa)}{qaK_1(qa)} + \frac{1}{h^2a^2} \\ &-\left[\left(\frac{n_1^2-n_2^2}{2n_1^2}\right)^2\left(\frac{K_1'(qa)}{qaK_1(qa)}\right)^2 + \left(\frac{\beta}{n_1 k}\right)^2\left(\frac{1}{h^2a^2}+\frac{1}{q^2a^2}\right)^2\right]^{1/2},\end{aligned}$$

where J_m are Bessel functions of the first kind, K_m are modified Bessel functions of the second kind, $k = \omega/c$, and

$$h = \sqrt{n_1^2k^2 - \beta^2}, \qquad q = \sqrt{\beta^2 - n_2^2k^2},$$

. We note that there are four different field distributions for the fundamental mode HE_{11}: two with opposite directions of propagation and two with opposite circular polarizations. In what follows, we write the field distribution for a guided mode with positive propagation constant and positive circular polarization using decomposition over cylindrical unit vectors

$$\widetilde{\mathbf{e}} = \mathbf{e}_r \widetilde{e}_r + \mathbf{e}_\varphi \widetilde{e}_\varphi + \mathbf{e}_z \widetilde{e}_z.$$

The cylindrical components of a normalized electric field amplitude for the HE_{11} mode in the core region are given by [27]

$$\begin{aligned}
\widetilde{e}_r &= iA\frac{q}{h}\frac{K_1(qa)}{J_1(ha)}\left[(1-s)J_0(hr) - (1+s)J_2(hr)\right], \\
\widetilde{e}_\varphi &= -A\frac{q}{h}\frac{K_1(qa)}{J_1(ha)}\left[(1-s)J_0(hr) + (1+s)J_2(hr)\right], \\
\widetilde{e}_z &= 2A\frac{q}{\beta}\frac{K_1(qa)}{J_1(ha)}J_1(hr),
\end{aligned}$$

and outside of the core region are given by

$$\begin{aligned}
\widetilde{e}_r &= iA\left[(1-s)K_0(qr) + (1+s)K_2(qr)\right], \\
\widetilde{e}_\varphi &= -A\left[(1-s)K_0(qr) - (1+s)K_2(qr)\right], \\
\widetilde{e}_z &= 2A\left(q/\beta\right)K_1(qr).
\end{aligned}$$

In the above equations s is a dimensionless parameter such that

$$s = \frac{1/h^2a^2 + 1/q^2a^2}{S},$$

where the denominator is as

$$S = J_1'(ha)/haJ_1(ha) + K_1'(qa)/qaK_1(qa),$$

The normalization constant defined from Eq. (A3) is

$$A = \frac{\beta}{2q}\frac{J_1\left(ha\right)/K_1\left(qa\right)}{\sqrt{2\pi a^2\left(n_1^2N_1 + n_2^2N_2\right)}}, \tag{A5}$$

where

$$\begin{aligned}
N_1 = \frac{\beta^2}{4h^2}\left\{(1-s)^2\left[J_0^2(ha) + J_1^2(ha)\right] + (1+s)^2\left[J_2^2(ha) - J_1(ha)J_3(ha)\right]\right\} \\
+ \frac{1}{2}\left[J_1^2(ha) - J_0(ha)J_2(ha)\right],
\end{aligned}$$

$$N_2 = \frac{J_1^2(ha)}{2K_1^2(qa)} \left\{ \frac{\beta^2}{2q^2} \left[(1-s)^2 \left[K_1^2(qa) - K_0^2(qa) \right] - (1+s)^2 \left[K_2^2(qa) - K_1(qa)K_3(qa) \right] \right] \right.$$
$$\left. - K_1^2(qa) + K_0(qa)K_2(qa) \right\}.$$

The intensity distribution of the electric field inside the core is defined by a quantity

$$|\widetilde{\mathbf{e}}(r)|^2 = 2A^2 \frac{K_1^2(qa)}{J_1^2(ha)} \left\{ \frac{q^2}{h^2} \left[(1-s)^2 J_0^2(hr) + (1+s)^2 J_2^2(hr) \right] + \frac{2q^2}{\beta^2} J_1^2(hr) \right\}, \qquad \text{(A6.a)}$$

and outside the core it is defined by the quantity

$$|\widetilde{\mathbf{e}}(r)|^2 = 2A^2 \left[(1-s)^2 K_0^2(qr) + (1+s)^2 K_2^2(qr) + \frac{2q^2}{\beta^2} K_1^2(qr) \right]. \qquad \text{(A6.b)}$$

Appendix B: Evaluation of the spontaneous decay rate into the fundamental guided mode

The following derivation of the spontaneous emission rate follows a standard approach based on the Hamiltonian for a system "two-level atom + vacuum field" given by

$$H = \hbar\omega_0 b^+ b + \sum_\lambda \hbar\omega_\lambda \left(a_\lambda^+ a_\lambda + \tfrac{1}{2} \right) - \mathbf{d}\cdot \sum_\lambda \left(\boldsymbol{\mathcal{E}}_\lambda b^+ a_\lambda + \boldsymbol{\mathcal{E}}_\lambda^* b a_\lambda^+ \right), \qquad \text{(B1)}$$

where b^+ and b are the atomic excitation and de-excitation operators, a^+ and a the creation and annihilation operators, and $\mathbf{d}$ is a matrix element of the atomic dipole moment. For the Hamiltonian (B1) the equations for probability amplitudes for the simplest case of a vacuum field initially in the vacuum state are

$$\dot{c}_{e,0} = \frac{i}{\hbar} \sum_\lambda \mathbf{d}\cdot\boldsymbol{\mathcal{E}}_\lambda \mathrm{e}^{-i\Delta_\lambda t} c_{g,1_\lambda}, \qquad \text{(B2.a)}$$

$$\dot{c}_{g,1_\lambda} = \frac{i}{\hbar} \mathbf{d}\cdot\boldsymbol{\mathcal{E}}_\lambda^* \mathrm{e}^{i\Delta_\lambda t} c_{e,0}, \qquad \text{(B2.b)}$$

where $c_{g,1_\lambda}$ are the probability amplitudes of the states which include the ground atomic state and the state of the vacuum field with one photon in mode λ and $c_{e,0}$ is a probability amplitude of the state which includes the excited atomic state and the state of the vacuum field with zero photon numbers in all the modes.

Taking a formal solution of the second equation in the above set

$$c_{g,1_\lambda} = \frac{i}{\hbar} \mathbf{d}\cdot\boldsymbol{\mathcal{E}}_\lambda^* \int_{t_0}^{t} \mathrm{e}^{i\Delta_\lambda t'} c_{e,0}(t') dt', \qquad \text{(B3.a)}$$

and substituting it into the first equation one can obtain an equation which describes the spontaneous decay of the upper atomic state

$$\dot{c}_{e,0} = -\frac{1}{\hbar^2}\sum_{\lambda}|\mathbf{d}\cdot\boldsymbol{\mathcal{E}}_{\lambda}|^2\int_{t_0}^{t}\mathrm{e}^{i\Delta_{\lambda}(t'-t)}c_{e,0}(t')dt'. \tag{B3.b}$$

An application of the above equation to the vacuum modes of free space gives a well-known decay equation

$$\dot{c}_{e,0} = -\gamma_0 c_{e,0}, \tag{B4}$$

where γ_0 is half the spontaneous decay rate into free space,

$$W_{\mathrm{sp}} = 2\gamma_0 = \frac{1}{4\pi\varepsilon_0}\frac{4d^2\omega_0^3}{3\hbar c^3}. \tag{B5}$$

We now apply basic equation (B3.b) to the fundamental guided mode HE_{11} of the vacuum field. The vacuum field of a single guided mode can be considered as periodic with spatial period, L, and the periodicity condition can be written as $\beta_\alpha L = 2\pi n_\alpha$, where $n_\alpha = 1, 2, 3, ...$ defines different values of the propagation constant, β_α. By making use of the periodicity condition, the sum over discrete numbers, n_α, in Eq. (B3.b) can be replaced by an integral such that

$$\sum \rightarrow \frac{L}{2\pi}\int d\beta.$$

Taking into account a one-to-one correspondence between values of the propagation constant and frequencies of the vacuum modes, $\beta = \beta(\omega)$, one can replace $d\beta$ by $d\beta = \widetilde{\beta}' d\omega$, where $\widetilde{\beta}' = d\beta/d\omega$. This gives

$$\sum \rightarrow \frac{L}{2\pi}\int \widetilde{\beta}' d\omega.$$

Next, integrating Eq. (B3.b) over frequency and time and using an equation

$$\int \mathrm{e}^{i(\omega-\omega_0)(t'-t)}d\omega = 2\pi\delta(t-t'),$$

while taking into account that the fundamental mode HE_{11} has two directions of propagation and two polarizations, Eq. (B3.b) can be rewritten as

$$\dot{c}_{e,0} = -\gamma^{(\mathrm{g})} c_{e,0}, \tag{B6}$$

where $\gamma^{(\mathrm{g})}$ is half the spontaneous decay rate into the guided mode

$$W_{\mathrm{sp}}^{(\mathrm{g})} = 2\gamma^{(\mathrm{g})} = \frac{\omega_0\widetilde{\beta}'}{\varepsilon_0\hbar}\left|\mathbf{d}\cdot\widetilde{\mathbf{e}}\right|^2. \tag{B7}$$

In the last equation $\widetilde{\mathbf{e}}$ is an amplitude of the guided mode with a positive propagation constant and positive circular polarization. Note that Eq. (B7) coincides with a corresponding equation from [4].

Assuming $d = d_+$ is a spherical component of the atomic dipole moment one can finally rewrite the spontaneous decay rate into the fundamental guided mode HE_{11} as

$$W_{\mathrm{sp}}^{(\mathrm{g})}(r) = 2\gamma^{(\mathrm{g})} = 2A^2 \frac{d^2\omega_0\widetilde{\beta}'}{\varepsilon_0\hbar}\left[(1-s)^2K_0^2(qr) + (1+s)^2K_2^2(qr) + \frac{2q^2}{\beta^2}K_1^2(qr)\right], \qquad \text{(B8)}$$

where the constant A is defined by Eq. (A5). Equation (B8) can be rewritten in a convenient form by introducing a dimensionless derivative, $\beta' = d\beta/dk = c\widetilde{\beta}'$, and making use of Eq. (B5) for the spontaneous decay rate into free space,

$$W_{\mathrm{sp}}^{(\mathrm{g})}(r) = 2\gamma^{(\mathrm{g})} = \gamma_0 \frac{3A^2\lambda^2\beta'}{\pi}\left[(1-s)^2K_0^2(qr) + (1+s)^2K_2^2(qr) + \frac{2q^2}{\beta^2}K_1^2(qr)\right]. \qquad \text{(B9)}$$

---

[1] H. Nha and W. Jhe, Phys. Rev. A **56**, 2213 (1997).

[2] T. Søndergaard and B. Tromborg, Phys. Rev. A **64**, 033812 (2001).

[3] V. V. Klimov and M. Ducloy, Phys. Rev. A **69**, 013812 (2004).

[4] Fam Le Kien, S. Dutta Gupta, V. I. Balykin, and K. Hakuta, Phys. Rev. A **72**, 032509 (2005).

[5] G. Sagué, E. Vetsch, W. Alt, D. Meschede, and A. Rauschenbeutel, Phys. Rev. Lett. **99**, 163602 (2007).

[6] K. P. Nayak, P. N. Melentiev, M. Morinaga, Fam Le Kien, V. I. Balykin, and K. Hakuta, Opt. Express **15**, 5431 (2007).

[7] M. A. Nielsen and I. L. Chuang, *Quantum computation and quantum information* (Cambridge Univ. Press, 2000).

[8] G. Alber, T. Beth, M. Horodecki, P. Horodecki, R. Horodecki, M. Rotteler, H. Weinfurter, R. Werner, A. Zeilinger, *Quantum information: An introduction to basic theoretical concepts and experiments*, Springer Tracts in Modern Physics, Vol. 173, Springer-Verlag (2001).

[9] J. P. Dowling and J. Gea-Banacloche, Adv. At. Mol. Opt. Phys. **36**, 1 (1996).

[10] V. I. Balykin, K. Hakuta, Fam Le Kien, J. Q. Liang, and M. Morinaga, Phys. Rev. A **70**, 011401(R) (2004).

[11] G. Sagu, A. Baade, and A. Rauschenbeutel, New. J. Phys. **10**, 113008 (2008).

[12] M. Cai, O. Painter, and K. J. Vahala, Phys. Rev. Lett. **85**, 74 (2000).

[13] J. Ward, D. O'Shea, B. Shortt, M. Morrissey, K. Deasy, and S. Nic Chormaic, Rev. Sci.Instrum. **77**, 083105 (2006).

[14] K. P. Nayak and K. Hakuta, New J. Phys. **10**, 053003 (2008).

[15] Fam Le Kien and K. Hakuta, Phys. Rev. A **75**, 013423 (2007).

[16] Yu. S. Barash and V. L. Ginzburg, Usp. Phys. Nauk **143**, 360 (1984).

[17] M. Oria, M. Chevrollier, D. Bloch, M. Fichet, and M. Ducloy, Europhys. Lett. **14**, 527 (1999).

[18] I. E. Dzyaloshinskii, E. M. Lifshitz, and L. Pitaevskii, Adv. Phys. **10**, 165 (1961).

[19] I. E. Dzyaloshinskii, E. M. Lifshitz, and L. P. Pitaevskii, Usp. Fiz. Nauk **73**, 381 (1961).

[20] Yoel Tikochinsky and Larry Spruch, Phys. Rev. A **48**, 4223 (1993).

[21] M. Fichet, F. Schuller, D. Bloch, and M. Ducloy, Phys. Rev. A **51**, 1553 (1995).

[22] H. J. Metcalf and P. van der Straten, Laser Cooling and Trapping, Springer-Verlag (1999).

[23] A. Krishna, K. Pandy, A. Wasan, and V. Natarajan, Europhys. Lett. **72**, 221 (2005).

[24] M. Chevrollier, D. Bloch, G. Rahmat, and M. Ducloy, Opt. Lett. **16**, 1879 (1991).

[25] W. R. Johnson, V. A. Dzuba, U. I. Safronova, and M. S. Safronova, Phys. Rev. A **69**, 022508 (2004).

[26] R. Loudon, *The Quantum Theory of Light* (Clarendon, Oxford, 1973).

[27] A. W. Snyder and J. D. Love, *Optical Waveguide Theory* (Chapman and Hall, New York, 1983).

[28] S. Chang and V. Minogin, Physics Reports **365**, 65 (2002).